J|A|C|S ARTICLES

Published on Web 02/22/2010

A Rare Example of a Krypton Difluoride Coordination Compound: $[BrOF_2][AsF_6]\cdot 2KrF_2$

David S. Brock,[†] Jonathan J. Casalis de Pury,[†] Hélène P. A. Mercier,[†] Gary J. Schrobilgen,*[,†] and Bernard Silvi[‡]

Department of Chemistry, McMaster University, Hamilton, Ontario L8S 4M1, Canada, and Laboratoire de Chimie Théorique (UMR-CNRS 7616), Université Pierre et Marie Curie-Paris 06, 4 place Jussieu, 75252 Paris cédex, France

Received November 20, 2009; E-mail: schrobil@mcmaster.ca

Abstract: The synthesis of $[BrOF_2][AsF_6]\cdot 2KrF_2$, its structural characterization, and bonding are described in this study. Although several KrF_2 adducts with transition metal centers have been previously reported, none have been crystallographically characterized. The solid-state Raman spectrum of $[BrOF_2][AsF_6]\cdot 2KrF_2$ has been assigned with the aid of quantum-chemical calculations. The low-temperature (−173 °C) X-ray crystal structure of $[BrOF_2][AsF_6]\cdot 2KrF_2$ consists of isolated molecular units and represents an example of KrF_2 coordinated to a main-group atom. The coordination geometry around the $BrOF_2^+$ cation renders the free valence electron lone pair more compact than in free $BrOF_2^+$. The KrF_2 ligands are coordinated trans to the fluorine atoms of $BrOF_2^+$ with the AsF_6^- anion coordinated trans to oxygen. The quantum theory of atoms in molecules (QTAIM) and electron localization function (ELF) analyses have been carried out in order to define the nature of the bonding in the complex. A significant amount of charge (0.25 e) is transferred to $BrOF_2^+$ from the two KrF_2 ligands (0.10 e each) and from the AsF_6^- anion (0.05 e). Significant polarization also occurs within the KrF_2 ligands, which enhances the anionic characters of the fluorine bridges. The interaction energy is mostly governed by the electrostatic interaction of the positively charged bromine atom with the surrounding fluorine atoms.

Introduction

The precursor to all known krypton compounds, KrF_2, has been structurally well characterized[1] and has been the subject of several theoretical studies.[2,3] The chemistry of krypton is restricted to the +2 oxidation state, presently consisting of several KrF^+ and $Kr_2F_3^+$ salts;[4−12] $Kr(OTeF_5)_2$;[13] a number of nitrile adducts of KrF^+, namely, $FKrN{\equiv}CR^+$ (R = H, CF_3, C_2F_5, n-C_3F_7);[14,15] preliminary evidence but no structural characterization for $KrF_2\cdot VF_5$[16] and $KrF_2\cdot MnF_4$,[17] and a series of KrF_2 Lewis acid−base adducts with group 6 d^0 transition metal centers, namely, $MOF_4\cdot KrF_2$ (M = Cr,[18] Mo,[19] W[19]). The structural characterizations of the latter KrF_2 adducts were limited to solution ^{19}F NMR and solid-state Raman spectroscopy. In all three cases, the Raman and ^{19}F NMR spectra indicate that the adducts result from weak coordination of KrF_2 through a fluorine bridge to the metal atom. In the absence of X-ray crystal structures, an assessment of the degree of coordination, based on the relative bond lengths of terminal and bridge Kr−F bonds, could not be made.

To date, there is no X-ray crystal structure in which KrF_2 serves as a ligand toward a metal atom, nor are there any examples in which KrF_2 coordinates to a main-group atom. Two criteria are required for KrF_2 coordination: (1) KrF_2 must interact with a Lewis acid center that is not sufficiently strong to "completely" abstract a fluoride ion from KrF_2, and (2) the Lewis acid must be resistant to oxidation by the powerful oxidative fluorinator, KrF_2. These criteria are met in the aforementioned low-temperature studies of the $MOF_4\cdot KrF_2$

[†] McMaster University.
[‡] Université Pierre et Marie Curie.

(1) Lehmann, J. F.; Mercier, H. P. A.; Schrobilgen, G. J. *Coord. Chem. Rev.* **2002**, *233*−*234*, 1–39.
(2) MacDougall, P. J.; Schrobilgen, G. J.; Bader, R. F. W. *Inorg. Chem.* **1989**, *28*, 763–769.
(3) Lehmann, J. F.; Dixon, D. A.; Schrobilgen, G. J. *Inorg. Chem.* **2001**, *40*, 3002–3017.
(4) Selig, H.; Peacock, R. D. *J. Am. Chem. Soc.* **1964**, *86*, 3895.
(5) Frlec, B.; Holloway, J. H. *J. Chem. Soc., Chem. Commun.* **1973**, 370–371.
(6) Frlec, B.; Holloway, J. H. *J. Chem. Soc., Chem. Commun.* **1974**, 89–90.
(7) Gillespie, R. J.; Schrobilgen, G. J. *J. Chem. Soc., Chem. Commun.* **1974**, 90–92.
(8) Holloway, J. H.; Schrobilgen, G. J. *J. Chem. Soc., Chem. Commun.* **1975**, 623–624.
(9) Frlec, B.; Holloway, J. H. *Inorg. Chem.* **1976**, *15*, 1263–1270.
(10) Gillespie, R. J.; Schrobilgen, G. J. *Inorg. Chem.* **1976**, *15*, 22–31.
(11) Gillespie, R. J.; Martin, D.; Schrobilgen, G. J. *J. Chem. Soc., Dalton Trans.* **1980**, 1898–1903.
(12) Selig, H.; Holloway, J. H. In *Topics in Current Chemistry*; Boschke, F. L., Ed.; Springer-Verlag: Berlin, 1984; Vol. 124, pp 33−90.
(13) Sanders, J. C. P.; Schrobilgen, G. J. *J. Chem. Soc., Chem. Commun.* **1989**, *20*, 1576–1578.
(14) Schrobilgen, G. J. *J. Chem. Soc., Chem. Commun.* **1988**, 863–865.
(15) Schrobilgen, G. J. *J. Chem. Soc., Chem. Commun.* **1988**, 1506–1508.
(16) Žemva, B.; Slivnik, J.; Šmalc, A. *J. Fluorine Chem.* **1975**, *6*, 191–193.
(17) Lutar, K.; Jesih, A.; Žemva, B. *Polyhedron* **1988**, *7*, 1217–1219.
(18) Christe, K. O.; Wilson, W. W.; Bougon, R. A. *Inorg. Chem.* **1986**, *25*, 2163–2169.
(19) Holloway, J. H.; Schrobilgen, G. J. *Inorg. Chem.* **1981**, *20*, 3363–3368.

adducts.[18,19] Earlier studies have shown that the $BrOF_2^+$ cation meets these criteria for the less strongly oxidizing XeF_2 ligand in $[BrOF_2][AsF_6]\cdot XeF_2$,[20] which has been characterized in solution by ^{19}F and ^{129}Xe NMR spectroscopy and in the solid state by Raman spectroscopy, offering promise for the synthesis of a KrF_2 analogue.

The present study extends the little studied coordination chemistry of krypton to the synthesis and characterization of the first main-group coordination compound of KrF_2, namely, $[BrOF_2][AsF_6]\cdot 2KrF_2$. In addition to structural characterization by solid-state Raman spectroscopy and single-crystal X-ray diffraction, the nature of the adduct bonding is examined using quantum-chemical calculations in conjunction with electron localization function (ELF) analyses.

Results and Discussion

Synthesis and Properties of $[BrOF_2][AsF_6]\cdot 2KrF_2$. Reaction progress and the purities of all products were routinely monitored by recording the low-temperature Raman spectra (−150 °C) of the solids.

The $[BrOF_2][AsF_6]\cdot XeF_2$ adduct was synthesized as previously described.[20] Rather than through the direct combination of $BrOF_3$ and AsF_5, the salt, $[BrOF_2][AsF_6]$, was synthesized in high purity by removal of XeF_2 from $[BrOF_2][AsF_6]\cdot XeF_2$ under dynamic vacuum at 0 °C (eq 1). This synthetic route to $[BrOF_2][AsF_6]$ circumvents difficulties associated with the synthesis and isolation of $BrOF_3$ from the reaction of $K[BrOF_4]$ and $[O_2][AsF_6]$ in HF[21,22] and the possibility of explosion during the hydrolysis of BrF_5 to form $BrOF_3$.[23]

$$[BrOF_2][AsF_6]\cdot XeF_2 \xrightarrow[0\ ^\circ C]{\text{dynamic vac}} [BrOF_2][AsF_6] + XeF_2 \quad (1)$$

Addition of KrF_2 to $[BrOF_2][AsF_6]$ (2:1 molar ratio) that had been precipitated and suspended in anhydrous HF (aHF) at −78 °C resulted in a significant volume increase with respect to the original volume of suspended $[BrOF_2][AsF_6]$. The Raman spectra of the solid product under frozen HF solvent and of the product isolated by removal of HF at −78 °C were identical. Both spectra revealed that the bands corresponding to $BrOF_2^+$ were shifted to lower frequencies relative to those of $[BrOF_2][AsF_6]$ and that the KrF_2 stretching band, associated with uncomplexed KrF_2, was replaced by two pairs of Kr−F stretching bands (see Raman Spectroscopy). The spectrum was consistent with the formation of $[BrOF_2][AsF_6]\cdot 2KrF_2$ according to eq 2. The adduct is stable for at least 5 days at −78 °C as a solid and under aHF solvent. The adduct is also stable in aHF up to 25 °C for at least 1 h, with Raman spectroscopy showing no discernible decomposition when the adduct was isolated by removal of the solvent under dynamic vacuum at −78 °C.

$$[BrOF_2][AsF_6] + 2KrF_2 \xrightarrow[12\ h,\ -78\ ^\circ C]{\text{HF}} [BrOF_2][AsF_6]\cdot 2KrF_2 \quad (2)$$

Attempts to form the 1:1 adduct, $[BrOF_2][AsF_6]\cdot KrF_2$, by reaction of a 1:1 molar ratio of $[BrOF_2][AsF_6]$ and KrF_2 in aHF at −78 °C yielded only a mixture of $[BrOF_2][AsF_6]\cdot 2KrF_2$ and $[BrOF_2][AsF_6]$ upon removal of the solvent under dynamic vacuum at −78 °C. Similar attempts to form a 3:1 adduct yielded only $[BrOF_2][AsF_6]\cdot 2KrF_2$ and unreacted KrF_2.

Table 1. Summary of Crystal Data and Refinement Results for $[BrOF_2][AsF_6]\cdot 2KrF_2$

chem formula	$AsBrOF_{12}Kr_2$
space group	$P2_1/c$ (No. 14)
a (Å)	5.7166(6)
b (Å)	13.644(1)
c (Å)	15.105(2)
β (deg)	111.446(4)
V (Å^3)	1096.6(2)
Z (molecules/unit cell)	4
mol wt (g mol^{-1})	2265.72
ρ_{calc} (g cm^{-3})	3.431
T (°C)	−173
μ (mm^{-1})	14.91
λ (Å)	0.71073
R_1[a]	0.0693
wR_2[b]	0.1715

[a] $R_1 = \sum||F_o| - |F_c||/\sum|F_o|$ for $I > 2\sigma(I)$. [b] wR_2 is defined as $\{\sum[w(F_o^2 - F_c^2)^2]/\sum w(F_o^2)^2\}^{1/2}$ for $I > 2\sigma(I)$.

X-ray Crystal Structure of $[BrOF_2][AsF_6]\cdot 2KrF_2$. A summary of the refinement results and other crystallographic information are given in Table 1. Important bond lengths, bond angles, and contacts are listed in Table 2.

The structure of $[BrOF_2][AsF_6]\cdot 2KrF_2$ consists of a $BrOF_2^+$ cation that interacts by means of short Br---F contacts with a single fluorine atom of the AsF_6^- anion and a fluorine atom from each of two KrF_2 ligands (Figure 1a). The $[BrOF_2][AsF_6]\cdot 2KrF_2$ structural units are relatively isolated, with the shortest intermolecular contacts (3.134−3.404 Å) occurring between the fluorine and krypton atoms of neighboring KrF_2 molecules, which are near or slightly under the sum of the fluorine and krypton van der Waals radii (3.49).[24]

The primary coordination sphere of Br(V) in $BrOF_2^+$ is trigonal pyramidal. The secondary coordination sphere comprises a fluorine atom of the AsF_6^- anion coordinated trans to the oxygen atom of $BrOF_2^+$ and the fluorine atoms of two KrF_2 molecules coordinated trans to the fluorine atoms of $BrOF_2^+$ so that the geometry of the F_2OBrF_3 moiety is pseudo-octahedral.

The Kr−F bond lengths of both coordinated KrF_2 molecules are distorted relative to those of free KrF_2 (1.894(5) Å),[3] with elongated bridge bonds (1.943(4), 1.933(4) Å) and terminal bonds that are shortened by nearly equal amounts (1.840(5), 1.847(4) Å). The differences between the terminal and bridging Kr−F bond lengths are significantly less than in KrF^+ and $Kr_2F_3^+$ salts: $[KrF][AsF_6]$ (Kr−F_b, 2.131(2) Å; Kr−F_t, 1.765(2) Å),[3] $[Kr_2F_3][AsF_6]\cdot[KrF][AsF_6]$ (Kr−F_b, 2.061(6), 2.049(6), 2.106(6) Å; Kr−F_t, 1.780(7), 1.803(6), 1.783(6) Å),[3] $[KrF][SbF_6]$ (Kr−F_b, 2.140(3) Å; Kr−F_t, 1.765(3) Å),[3] $[KrF][BiF_6]$ (Kr−F_b, 2.090(6) Å; Kr−F_t, 1.774(6) Å),[3] $[Kr_2F_3]_2[SbF_6]_2\cdot KrF_2$ (Kr−F_b, 2.041(4), 2.065(4), 2.052(5), 2.056(4) Å; Kr−F_t, 1.805(5), 1.799(4), 1.797(5), 1.787(4) Å),[3] and $[Kr_2F_3][SbF_6]\cdot KrF_2$ (Kr−F_b, 2.027(5), 2.046(5) Å; Kr−F_t, 1.800(5), 1.790(5) Å).[3] This indicates that the Kr−F_b bonds in $[BrOF_2][AsF_6]\cdot 2KrF_2$ have considerably more covalent character relative to those of KrF^+ and $Kr_2F_3^+$ salts and that the KrF_2 molecules behave as coordinating ligands rather than as fluoride ion donors.

The KrF_2 molecules coordinate to the cation by means of Br---F(3) and Br---F(5) contacts of 2.318(4) and 2.356(4) Å,

(20) Holloway, J. H.; Schrobilgen, G. J. *Inorg. Chem.* **1980**, *19*, 2632–2640.
(21) Bougon, R.; Bui Huy, T. *Compt. Rend.* **1976**, *C283*, 461–463.
(22) Gillespie, R. J.; Spekkens, P. *J. Chem. Soc., Dalton Trans.* **1977**, 1539–1546.
(23) Lehmann, J. F. Ph.D. Thesis, McMaster University, Hamilton, ON, 2004.
(24) Bondi, A. *J. Phys. Chem.* **1964**, *68*, 441–451.

Table 2. Experimental and Calculated (C_1) Geometrical Parameters for $[BrOF_2][AsF_6]\cdot 2KrF_2$

exptl[a]			PBE1PBE[a]	B3LYP[a]
		Bond Lengths (Å)		
Br(1)−O(1)	1.564(5)	Br(1)−O(1)	1.556	1.569
Br(1)−F(1)	1.727(4)	Br(1)−F(1)	1.731	1.757
Br(1)−F(2)	1.723(4)	Br(1)−F(2)	1.730	1.757
Br(1)---F(3)	2.318(4)	Br(1)---F(3)	2.350	2.363
Br(1)---F(5)	2.356(4)	Br(1)---F(5)	2.302	2.338
Br(1)---F(7)	2.576(4)	Br(1)---F(7)	2.579	2.529
Kr(1)−F(3)	1.943(4)	Kr(1)−F(3)	1.951	1.984
Kr(1)−F(4)	1.840(5)	Kr(1)−F(4)	1.814	1.843
Kr(2)−F(5)	1.933(4)	Kr(2)−F(5)	1.957	1.984
Kr(2)−F(6)	1.847(4)	Kr(2)−F(6)	1.808	1.837
As(1)−F(7)	1.742(4)	As(1)−F(7)	1.789	1.813
As(1)−F(8)	1.711(4)	As(1)−F(8)	1.709	1.722
As(1)−F(9)	1.732(4)	As(1)−F(9)	1.743	1.752
As(1)−F(10)	1.732(4)	As(1)−F(10)	1.724	1.742
As(1)−F(11)	1.712(4)	As(1)−F(11)	1.705	1.720
As(1)−F(12)	1.709(4)	As(1)−F(12)	1.761	1.773
		Bond Angles (deg)		
F(1)−Br(1)−F(2)	89.3(2)	F(1)−Br(1)−F(2)	89.1	89.8
F(1)−Br(1)−O(1)	103.3(3)	F(1)−Br(1)−O(1)	102.0	102.0
F(1)−Br(1)---F(3)	85.1(2)	F(1)−Br(1)---F(3)	83.9	85.7
F(1)−Br(1)---F(5)	162.4(2)	F(1)−Br(1)---F(5)	166.9	166.5
F(1)−Br(1)---F(7)	80.5(2)	F(1)−Br(1)---F(7)	89.9	86.1
F(2)−Br(1)−O(1)	102.8(3)	F(2)−Br(1)−O(1)	100.0	100.1
F(2)−Br(1)---F(3)	166.7(2)	F(2)−Br(1)---F(3)	172.5	173.7
F(2)−Br(1)---F(5)	84.9(2)	F(2)−Br(1)---F(5)	82.4	83.4
F(2)−Br(1)---F(7)	83.5(2)	F(2)−Br(1)---F(7)	72.1	74.1
O(1)−Br(1)---F(3)	90.2(2)	O(1)−Br(1)---F(3)	84.1	85.3
O(1)−Br(1)---F(5)	94.2(2)	O(1)−Br(1)---F(5)	89.3	90.7
O(1)−Br(1)---F(7)	172.6(2)	O(1)−Br(1)---F(7)	165.7	170.2
F(3)−Kr(1)−F(4)	179.9(2)	F(3)−Kr(1)−F(4)	177.2	176.9
F(3)---Br(1)---F(5)	96.9(2)	F(3)---Br(1)---F(5)	104.0	100.1
F(3)---Br(1)---F(7)	83.7(2)	F(3)---Br(1)---F(7)	105.3	101.1
F(5)−Kr(2)−F(6)	178.7(2)	F(5)−Kr(2)−F(6)	177.5	177.7
F(5)---Br(1)---F(7)	82.3(2)	F(5)---Br(1)---F(7)	78.0	80.8
Br(1)---F(3)−Kr(1)	132.1(2)	Br(1)---F(3)−Kr(1)	138.9	139.6
Br(1)---F(5)−Kr(2)	139.9(2)	Br(1)---F(5)−Kr(2)	129.4	129.4
Br(1)---F(7)−As(1)	131.1(2)	Br(1)---F(7)−As(1)	114.8	123.7
F(7)−As(1)−F(8)	179.4(2)	F(7)−As(1)−F(8)	175.8	176.6
F(7)−As(1)−F(9)	89.1(2)	F(7)−As(1)−F(9)	86.8	87.4
F(7)−As(1)−F(10)	88.8(2)	F(7)−As(1)−F(10)	88.6	87.9
F(7)−As(1)−F(11)	88.4(4)	F(7)−As(1)−F(11)	90.1	89.6
F(7)−As(1)−F(12)	89.5(2)	F(7)−As(1)−F(12)	85.6	85.6
F(8)−As(1)−F(9)	90.4(2)	F(8)−As(1)−F(9)	91.5	91.9
F(8)−As(1)−F(10)	91.6(2)	F(8)−As(1)−F(10)	92.9	92.6
F(8)−As(1)−F(11)	91.2(2)	F(8)−As(1)−F(11)	93.8	93.8
F(8)−As(1)−F(12)	90.8(2)	F(8)−As(1)−F(12)	90.5	91.0
F(9)−As(1)−F(10)	177.9(2)	F(9)−As(1)−F(10)	174.5	174.5
F(9)−As(1)−F(11)	90.4(2)	F(9)−As(1)−F(11)	91.1	91.2
F(9)−As(1)−F(12)	89.1(2)	F(9)−As(1)−F(12)	87.6	87.9
F(10)−As(1)−F(11)	90.1(2)	F(10)−As(1)−F(11)	91.9	91.6
F(10)−As(1)−F(12)	90.4(2)	F(10)−As(1)−F(12)	89.1	88.9
F(11)−As(1)−F(12)	177.8(2)	F(11)−As(1)−F(12)	175.5	175.1

[a] The aug-cc-pVTZ(-PP) basis set was used. The symmetry of the energy-minimized geometry is C_1. The labeling scheme corresponds to that used in Figure 1a and b.

respectively, which are relatively short and significantly less than the sum of the van der Waals radii of Br and F (3.32 Å). The fluorine bridges, Br(1)---F(3)−Kr(1) and Br(1)---F(5)−Kr(2), are bent as a consequence of the AX_2E_2 VSEPR[25] arrangement of bond pair and electron lone pair domains of the bridging fluorine atom, resulting in angles of 132.1(2)° and 139.9(2)°, respectively (also see the Supporting Information). The Br---F_b−Kr angles appear to be little influenced by steric interactions, with $F_b\cdots F_b$ distances of 3.25−3.50 Å and $F_b\cdots F_{Br}$ distances of 2.77−2.93 Å compared to the van der Waals sum of 2.94 Å.[24] The only other short intramolecular contacts are Kr(1)---F(9) (3.22 Å) and Kr(2)---F(10) (3.40 Å), which are near the van der Waals sum for krypton and fluorine (3.49 Å). The KrF_2 ligands retain their linearity with F(3)−Kr(1)−F(4) and F(5)−Kr(2)−F(6) angles of 179.9(2)° and 178.7(2)°, respectively. One fluorine atom of the AsF_6^- anion forms a relatively short Br---F_b bridge bond (2.576(4) Å) with the $BrOF_2^+$ cation, giving rise to a distorted octahedral arrangement around arsenic in which the As−F_b bond (1.742(4) Å) is elongated relative to the As−F bond trans to it (1.711(4) Å) and the equatorial bonds, which range in length from 1.709(4) to 1.732(4) Å.

(25) Gillespie, R. J.; Hargittai, I. In *The VSEPR Model of Molecular Geometry*; Allyn and Bacon: Boston, MA, 1991; pp 154−155.

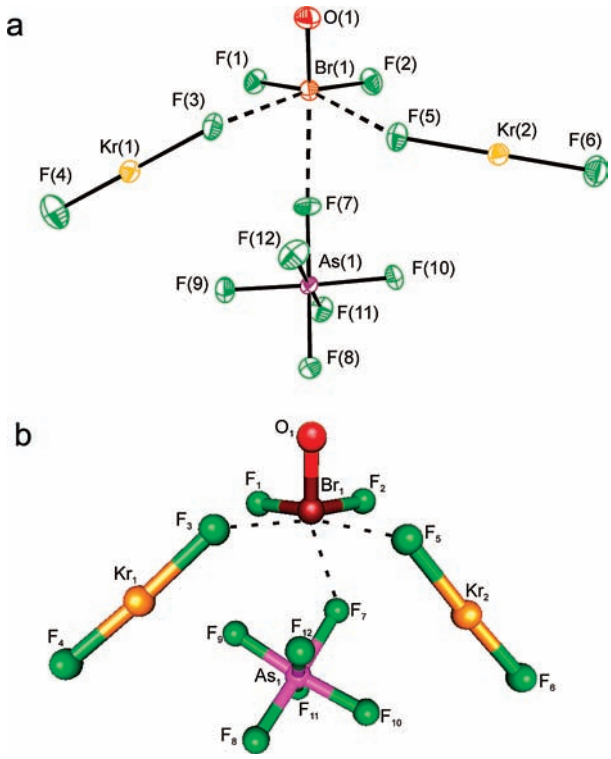

Figure 1. (a) Structural unit in the X-ray crystal structure of $[BrOF_2][AsF_6]\cdot 2KrF_2$; thermal ellipsoids are shown at the 50% probability level. (b) Calculated geometry (PBE1PBE/aug-cc-pVTZ(-PP)) of $[BrOF_2][AsF_6]\cdot 2KrF_2$ showing the pseudo-octahedral coordination around bromine(V).

The Br−O bond length (1.564(5) Å) is equal, within $\pm 3\sigma$, to that of $BrOF_4^-$ in $[NO][BrOF_4]$ (1.575(3) Å)[26] and the neutral parent molecule, $BrOF_3$, in $[NO_2][BrF_4]\cdot 2BrOF_3$ (1.569, 1.606 Å)[26] but is significantly shorter than in the neutral species $O_2Br-O-BrO_2$ (1.606 (12), 1.611(2), 1.613(2), 1.606(2) Å)[27] and $O_2BrOTeF_5$ (1.595(4), 1.608(3) Å)[28] and in the BrO_2^+ cation of $[BrO_2][SbF_6]$ (1.595(2) Å).[29] The Br−O bond length is also comparable to the Se−O bond length in isoelectronic $SeOF_2$ (1.576 Å), which was measured in the gas phase by microwave spectroscopy.[30] The Br−F bond lengths in $[BrOF_2][AsF_6]\cdot 2KrF_2$ (1.727(4), 1.723(4) Å) are equal, within $\pm 3\sigma$, to the axial Br−F bond lengths of the BrF_4^+ cation in $[BrF_4][Sb_2F_{11}]$ (Br−F_{ax}, 1.728(3), 1.729(3) Å (Br−F_{eq}, 1.664(3), 1.667(2) Å)),[31] the equatorial Br−F bond lengths in the neutral parent molecule, $BrOF_3$, in $[NO_2][BrF_4]\cdot 2BrOF_3$ (Br−F_{ax}, 1.820, 1.839, 1.822, 1.836 Å; Br−F_{eq}, 1.725, 1.692 Å),[26] and the Se−F bond lengths of the isoelectronic $SeOF_2$ molecule (1.7295 Å).[30] They are, however, significantly shorter than the Br−F bonds in $[NO][BrOF_4]$ (1.846(2), 1.912(2) Å).[26]

The valence electron lone pair of bromine in $[BrOF_2][AsF_6]\cdot 2KrF_2$ is expected to occupy a region opposite the three primary bond domains, giving a tetrahedral AX_2YE VSEPR[25] arrangement at Br(V). Thus, a stereochemically active valence electron lone pair is expected to occupy a region at the center of the triangular arrangement defined by the three long contacts that comprise the more open face of the pseudo-octahedron. The sum of the F(3)---Br(1)---F(5) (96.9(2)°), F(3)---Br(1)---F(7) (83.7(2)°), and F(5)---Br(1)---F(7) (82.3(2)°) angles is 262.9(6)°, whereas the face of the octahedron containing the primary contacts is significantly more open (F(1)−Br(1)−O(1), 103.3(3)°; F(1)−Br(1)−F(2), 89.3(2)°; F(2)−Br(1)−O(1), 102.8(3)°) with an angle sum of 295.4(8)°. The angle sums are attributable to the greater steric requirement of the Br−O double bond domain. The short secondary contact distances observed in $[BrOF_2][AsF_6]\cdot 2KrF_2$ render the valence electron lone pair domain of bromine more compact and localized around the bromine atom relative to that of free $BrOF_2^+$. The steric crowding of the Br(V) valence electron lone pair represents an example of a "weakly active" electron lone pair[32] (see Computational Results).

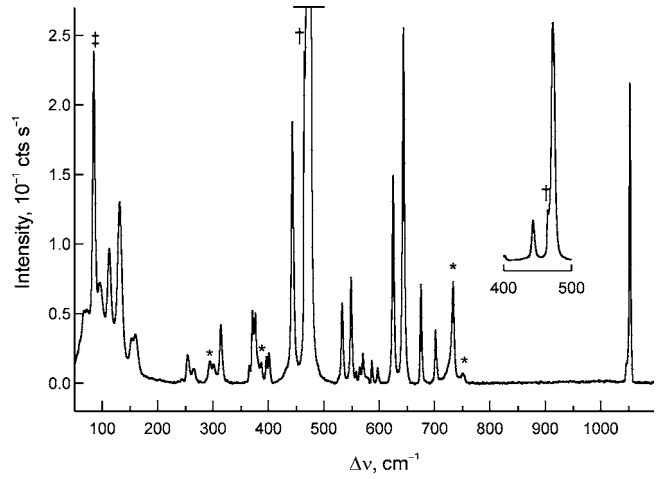

Figure 2. Raman spectrum of $[BrOF_2][AsF_6]\cdot 2KrF_2$ recorded at −150 °C using 1064 nm excitation. Symbols denote FEP sample tube lines (∗), unreacted KrF_2 (†), and instrumental artifact (‡).

Raman Spectroscopy. The low-temperature Raman spectrum of $[BrOF_2][AsF_6]\cdot 2KrF_2$ is shown in Figure 2. The observed and calculated frequencies and their detailed assignments are listed in Table 3. The spectral assignments for $[BrOF_2][AsF_6]\cdot 2KrF_2$ were made by comparison with the calculated vibrational frequencies and Raman intensities (Table 3) of the energy-minimized geometry (Figure 1b), as well as those of KrF_2 (Table S2 in the Supporting Information). In both the crystal structure and the calculated geometry, the $[BrOF_2][AsF_6]\cdot 2KrF_2$ structural unit possesses C_1 symmetry and the Raman spectrum has been assigned under that symmetry. Vibrational frequencies calculated at both the PBE1PBE and B3LYP (values in parentheses) levels of theory reproduced the observed frequency trends. The AsF_6^- anion, under ideal octahedral symmetry (O_h), has three Raman-active bands, $\nu_1(A_{1\,g})$, $\nu_2(E_g)$, and $\nu_5(T_{2g})$, two infrared-active bands, $\nu_3(T_{1u})$ and $\nu_4(T_{1u})$, and one inactive band, $\nu_6(T_{2u})$. In the present instance, the fluorine-bridged AsF_6^- anion is distorted, with local C_1 symmetry which gives rise to 15 Raman- and infrared-active bands. Only eight bands were observed in the Raman spectrum of AsF_6^- and their assignments were

(26) Ellern, A.; Boatz, J. A.; Christe, K. O.; Drews, T.; Seppelt, K. *Z. Anorg. Allg. Chem.* **2002**, *628*, 1991–1999.
(27) Leopold, D.; Seppelt, K. *Angew. Chem., Int. Ed. Engl.* **1994**, *33*, 975–976; *Angew. Chem.* **1994**, *106*, 1043−1044.
(28) Hwang, I.-C.; Kuschel, R.; Seppelt, K. *Z. Anorg. Allg. Chem.* **1997**, *623*, 379–383.
(29) Lehmann, J. F.; Riedel, S.; Schrobilgen, G. J. *Inorg. Chem.* **2008**, *47*, 8343–8356.
(30) Bowater, I. C.; Brown, R. D.; Burden, F. R. *J. Mol. Spectrosc.* **1968**, *28*, 461–470.
(31) Vij, A.; Tham, F. S.; Vij, V.; Wilson, W. W.; Christe, K. O. *Inorg. Chem.* **2002**, *41*, 6397–6403.
(32) Pilmé, J.; Robinson, E. A.; Gillespie, R. J. *Inorg. Chem.* **2006**, *45*, 6198–6204.

Table 3. Experimental and Calculated Vibrational Frequencies[a] for $[BrOF_2][AsF_6]\cdot 2KrF_2$

Experimental and Calculated Vibrational Frequencies[a] for $[BrOF_2][AsF_6]\cdot 2KrF_2$

exptl[b]	PBE1PBE[c]	B3LYP[c]	assgnts (C_1)[d] $[BrOF_2][AsF_6]\cdot 2KrF_2$	AsF_6^- (O_h)
1053(19) 1047(1)	1071(68)[69]	1021(80)[69]	ν(BrO)	
702(3)	745(6)[174]	718(6)[167]	$\nu(AsF_{11}) - \nu(AsF_{12})$	$\nu_3(T_{1u})$
	729(3)[165]	707(4)[157]	$\nu(AsF_8)$	
	724(<1)[232]	698(<1)[229]	$\nu(AsF_9) - \nu(AsF_{10})$	
675(6)	662(18)[71]	637(56)[45]	$\nu(AsF_7) + \nu(AsF_9) + \nu(AsF_{10}) + \nu(AsF_{12})$ [e]	$\nu_1(A_{1g})$
644(22)	683(58)[85]	644(32)[45]	$\nu(BrF_1) + \nu(BrF_2)$ [f]	
625(13)	652(26)[68]	612(31)[67]	$\nu(BrF_1) - \nu(BrF_2)$	
549(7)	610(28)[182]	577(20)[194]	$\nu(Kr_2F_6) + [\nu(Kr_1F_4) - \nu(BrF_1)]_{small}$	
533(5)	587(21)[295]	549(12)[295]	$\nu(Kr_1F_4) - [\nu(Kr_2F_6) + \nu(BrF_2)]_{small}$	
597(1) 587(1)	571(4)[6]	557(6)[70]	$[\nu(AsF_9) + \nu(AsF_{10})] - [\nu(AsF_{11}) + \nu(AsF_{12})]$	$\nu_2(E_g)$
565(1) 558(1)	536(5)[31]	504(20)[50]	$\nu(AsF_7) - \nu(AsF_{12})_{small}$	
472(100), br	489(76)[124]	473(87)[84]	$\nu(Kr_1F_3) + [\nu(Kr_2F_5) - \nu(AsF_7)]_{small}$	
443(17)	467(33)[270]	450(43)[231]	$\nu(Kr_2F_5) - \nu(Kr_1F_3)_{small}$	
401(2)	401(<1)[45]	391(<1)[49]	$\delta(F_9AsF_{12}) - \delta(F_{10}AsF_{11}) + \rho_w(F_7AsF_8)$	$\nu_4(T_{1u})$
	396(<1)[26]	385(<1)[32]	$\delta(F_8AsF_9) - \delta(F_7AsF_{10}) + \rho_w(F_{11}AsF_{12})$	
	394(<1)[39]	383(<1)[31]	$\delta(AsF_7F_9F_{11})_{oop} - \delta(AsF_8F_{10}F_{12})_{oop}$	
397(2)	386(4)[123]	368(4)[103]	$\delta(OBrF_1F_2)$	
366(1)	367(1)[<1]	359(1)[<1]	$\delta(F_9AsF_{12}) + \delta(F_{10}AsF_{11})$	$\nu_5(T_{2g})$
	362(1)[1]	352(1)[3]	$\delta(F_7AsF_{12}) + \delta(F_8AsF_{11})$	
	356(<1)[<1]	344(<1)[<1]	$\delta(F_7AsF_9) + \delta(F_8AsF_{10})$	
377(4) 371(5)	334(5)[84]	319(4)[69]	$\rho_w(OBrF_2) + \rho_t(F_1BrF_2)$	
314(4)	304(<1)[7]	283(<1)[9]	$\delta(F_1BrF_2)$	
301(1)	291(1)[44]	274(1)[34]	$\delta(F_5Kr_2F_6)_{oop}$	
266(1)	269(2)[67]	258(1)[53]	$\delta(F_3Kr_1F_4)_{ip}$	
254(2)	256(<1)[7]	243(<1)[8]	$\delta(F_5Kr_2F_6)_{ip}$	
	246(<0.1)[5]	241(<0.1)[4]	$\rho_w(F_7AsF_8) - \rho_w(F_9AsF_{10}) + [\delta(F_3Kr_1F_4)_{oop}]_{small}$	
	244(1)[9]	234(1)[12]	$\delta(F_3Kr_1F_4)_{oop} + [\rho_w(F_7AsF_8) - \rho_w(F_9AsF_{10})]_{small}$	$\nu_6(T_{2u})$
	235(<1)[<1]	227(<0.1)[<1]	$\rho_w(F_{11}AsF_{12}) - \rho_w(F_7AsF_8) + \rho_w(F_9AsF_{10})$	
	230(<0.1)[<1]	221(<0.1)[<1]	$\rho_w(F_9AsF_{10}) - \rho_w(F_{11}AsF_{12}) + \rho_w(F_7AsF_8)$	
161(3)	174(2)[5]	166(4)[5]	$\rho_r(OBrF_2) + \rho_t(F_5Kr_2F_6)$	
153(1)	169(2)[22]	165(<1)[19]	$\rho_t(F_1BrF_2) + \rho_t(F_5Kr_2F_6)$	
	148(<1)[7]	146(1)[9]	$\rho_t(OBrF_1F_2) + \rho_t(F_5Kr_2F_6)_{small}$	
	127(<1)[7]	119(1)[6]	$\rho_t(OBrF_1F_2)$	
	109(4)[27]	106(3)[16]	$\rho_r(OBrF_1F_2) + \rho_t(F_3Kr_1F_4)$	
	101(2)[1]	100(3)[2]	$\rho_r(F_5Kr_2F_6) - \rho_r(F_3Kr_1F_4) + \rho_t(OBrF_1F_2)_{small}$	
	89(2)[<1]	86(<1)[<1]	deformation and torsional modes of $[BrOF_2][AsF_6]\cdot 2KrF_2$	
	80(1)[5]	82(2)[2]		
	72(<1)[<1]	64(<1)[<1]		
	62(<1)[1]	61(1)[<1]		
	51(<1)[1]	48(<1)[<1]		
	48(<1)[<1]	44(<1)[<1]		
	42(2)[<1]	40(3)[<1]		
	39(<1)[<1]	33(<1)[1]		
	30(<1)[<1]	19(1)[<1]		
	22(1)[<1]	11(<0.1)[<1]		
132(11) 113(8) 96(6)			lattice modes	

[a] Frequencies are given in cm^{-1}. [b] The Raman spectrum was recorded in an FEP sample tube at −150 °C using 1064 nm excitation. Values in parentheses denote relative Raman intensities. An additional band observed at 465(21) cm^{-1} was assigned to unreacted KrF_2. The abbreviation br denotes broad. [c] The aug-cc-pVTZ(-PP) basis set was used. Values in parentheses denote Raman intensities ($Å^4\ u^{-1}$). Values in square brackets denote infrared intensities (km mol^{-1}). [d] Vibrational assignments were based on modes calculated at the PBE1PBE level of theory. The abbreviations denote stretch (ν), bend (δ), rock (ρ_r), twist (ρ_t), wag (ρ_w), in-plane bend (ip), and out-of-plane bend (oop). [e] This band is assigned to $\nu(BrF_1) + \nu(BrF_2)$ at the B3LYP level. [f] This band is assigned to $\nu(AsF_{13}) + \nu(AsF_{14}) + \nu(AsF_{10}) + \nu(AsF_9)$ at the B3LYP level.

guided by comparison with other coordinated AsF_6^- anions having local C_1 or C_s symmetries.[33,34]

All 45 vibrational modes of $[BrOF_2][AsF_6]\cdot 2KrF_2$ belong to A irreducible representations and are predicted to be Raman- and infrared-active. Additional bands appear in the Raman spectrum that cannot be accounted for by site symmetry lowering alone because correlation of the gas-phase adduct symmetry (C_1) to the crystal site symmetry (C_1) results in no additional band splitting (Table S1 in the Supporting Information). The additional bands are associated with vibrational coupling within the crystallographic unit cell. Correlation of the site symmetry to the centrosymmetric unit cell symmetry (C_{2h} with $Z = 4$) results in equal apportioning of the $4(3N - 6)$ vibrational modes among A_g, A_u, B_g, and B_u symmetries. Thus, of the 180 coupled vibrational modes for $[BrOF_2][AsF_6]\cdot 2KrF_2$

(33) Gerken, M.; Moran, M. D.; Mercier, H. P. A.; Pointner, B. E.; Schrobilgen, G. J.; Hoge, B.; Christe, K. O.; Boatz, J. A. *J. Am. Chem. Soc.* **2009**, *131*, 13474–13489.
(34) Smith, G. L.; Mercier, H. P. A.; Schrobilgen, G. J. *Inorg. Chem.* **2007**, *46*, 1369–1378.

in its unit cell, 45 A_g and 45 B_g Raman-active and 45 A_u and 45 B_u infrared-active components are predicted. Of the predicted 90 Raman bands, only 25, including eight AsF_6^- bands, were observed, implying vibrational coupling within the unit cell is, except in a few instances, too weak to be observed.

Upon coordination of KrF_2, the cation stretching frequencies shift to lower frequency relative to those of $[BrOF_2][AsF_6]$.[35] The highest frequency bands at 1047, 1053 cm^{-1} are assigned to the factor-group split Br−O stretching mode. The in-phase and out-of-phase BrF_2 stretching bands occur at 644 and 625 cm^{-1}, respectively, and show no factor-group splitting. The in-phase band occurs at higher frequency and is more intense, in agreement with the trends expected from the calculated values. The two bands are also slightly shifted to lower frequency compared to those observed for free $BrOF_2^+$.[35] The trends in the cation stretching frequencies can be accounted for by donation of electron density from the KrF_2 ligands to the bromine atom, rendering bromine less electropositive (see Natural Bond Orbital Analyses) and shifting the modes to lower frequency. The cation bands at 314, 371/377, and 397 cm^{-1} are assigned to $BrOF_2^+$ deformation modes and are in good agreement with the calculated values.

The most intense modes in the spectrum of $[BrOF_2][AsF_6]\cdot 2KrF_2$ are those of the KrF_2 ligand. Coordination of KrF_2 to $BrOF_2^+$ results in removal of the center of symmetry at krypton, which is manifested in the Raman spectrum by the appearance of bands to high and to low frequency of free KrF_2 (ν(KrF), 465 cm^{-1}),[36] with the higher frequency and more intense band assigned to the terminal Kr−F_t stretch and the lower frequency band assigned to the bridging Kr−F_b stretch. These trends have been observed in XeF_2 adducts with metal cations.[37,38] The vibrational displacements calculated at the PBE1PBE and B3LYP levels reveal that while there is no intraligand coupling for the Kr−F_t and Kr−F_b stretching modes, interligand coupling occurs giving rise to in-phase (KrF_t) + ν($Kr'F_t$) and out-of-phase (KrF_t) − ν($Kr'F_t$) modes at 549 and 533 cm^{-1}, respectively, where the KrF_t and $Kr'F_t$ displacement amplitudes are unequal in both coupled modes. These modes occur at similar frequencies, in accordance with their calculated frequencies at 610 (577) and 587 (549) cm^{-1}, respectively. The bands at 443 and 472 cm^{-1} are associated with analogous interligand coupling of the Kr−F_b bridging stretching modes and are in good agreement with the calculated values, 467 (450) and 489 (473) cm^{-1}. In contrast to the coupled Kr−F_t and $Kr'F_t$ modes, the coupled Kr−F_b and Kr′-F_b displacement amplitudes are nearly equal. The Kr−F_t stretching frequencies are comparable to ν(KrF_t) of $CrOF_4\cdot KrF_2$ (550 cm^{-1})[18] but are somewhat lower than those of $MoOF_4\cdot KrF_2$ (566, 579 cm^{-1})[19] and $WOF_4\cdot KrF_2$ (571, 581 cm^{-1}).[19] The value is, however, much lower than that of ν(KrF) in β-[KrF][AsF_6] (615, 619 cm^{-1})[3], [KrF][SbF_6] (615 cm^{-1})[3] and [KrF][BiF_6] (604, 610 cm^{-1}),[3] indicating that the coordinated KrF_2 molecules in $[BrOF_2][AsF_6]\cdot 2KrF_2$ are adducted and do not behave as fluoride ion donors toward the Lewis acid, $BrOF_2^+$, as inferred from their relative crystallographic bond lengths (see X-ray Crystallography).

The Kr−F_b bridging frequencies are in better agreement with those of $WOF_4\cdot KrF_2$ (450, 469 cm^{-1})[19] than with those of $CrOF_4\cdot KrF_2$ (486 cm^{-1})[18] or $MoOF_4\cdot KrF_2$ (462, 479 cm^{-1}).[19] Comparison of the frequency differences between the Kr−F_t and Kr−F_b modes reveals an increase over the series $CrOF_4\cdot KrF_2$ (64 cm^{-1}),[18] $MoOF_4\cdot KrF_2$ (102 cm^{-1}),[19] and $WOF_4\cdot KrF_2$ (116 cm^{-1}),[19] following the anticipated Lewis acidity trend of the metal oxide tetrafluorides. This trend suggests that the strengths of the Br---F adduct bonds in $[BrOF_2][AsF_6]\cdot 2KrF_2$, with a frequency difference between the Kr−F_t and Kr−F_b modes of 84 cm^{-1}, are intermediate with respect to those of $CrOF_4\cdot KrF_2$ and $MoOF_4\cdot KrF_2$.

The present vibrational assignments of coordinated KrF_2 are in accordance with those reported for XeF_2 homoleptically coordinated to a variety of metal cations.[37,38] In these coordination complexes, the high-frequency Xe−F stretching bands are assigned to Xe−F_t stretches and the low-frequency ones are assigned to Xe−F_b stretches without invoking intramolecular coupling in the vibrational mode descriptions of coordinated XeF_2. The calculated vibrational displacements of coordinated KrF_2 in $[BrOF_2][AsF_6]\cdot 2KrF_2$ also do not show intramolecular coupling. Instead, the vibrational coupling of the Kr−F stretches is interligand in nature occurring between Kr−F_b stretching modes that have near-equal displacement amplitudes and between Kr−F_t stretching modes that have unequal displacement amplitudes.

The double degeneracy of the KrF_2 bending mode of free KrF_2 (ν_2, Π_u) is removed when it is fluorine-bridged to bromine, resulting in splitting into out-of-plane and in-plane F_t−Kr−F_b bending modes with respect to the plane containing the two KrF_2 molecules and the bromine atom. The vibrational bands are shifted to higher frequency relative to that of free KrF_2 (236 cm^{-1})[39] and occur at slightly different frequencies because one KrF_2 ligand is somewhat more strongly bound than the other in the crystal structure and in the calculated gas-phase structure (see X-ray Crystal Structure and Computational Results). The δ(FKrF) modes are not coupled (Table 3), where $\delta(F_5KrF_6)_{ip}$ and $\delta(F_5KrF_6)_{oop}$ are observed at 254 and 301 cm^{-1}, respectively, and $\delta(F_3KrF_4)_{ip}$ is observed at 266 cm^{-1}. The $\delta(F_3KrF_4)_{oop}$ bend was not observed but is calculated at 244 (234) cm^{-1} and is expected to be weak. The calculated frequencies are also in excellent agreement with the experimental frequencies. These bands occur at much higher frequencies than those that are assigned for the MOF_4 adducts, i.e., 176 cm^{-1} ($CrOF_4\cdot KrF_2$),[18] 170 cm^{-1} ($MoOF_4\cdot KrF_2$),[19] and 172 cm^{-1} ($WOF_4\cdot KrF_2$),[19] suggesting that the latter may have been erroneously assigned in the earlier work and likely should be reassigned to the bands reported at 256/283, 303/312, and 301/312, respectively.

Computational Results. The geometry of $[BrOF_2][AsF_6]\cdot 2KrF_2$ was energy minimized starting from the crystallographic coordinates and resulted in stationary points with all frequencies real. The PBE1PBE/aug-cc-pVTZ(-PP) and B3LYP/aug-cc-pVTZ(-PP) (B3LYP values are in parentheses) results are reported in Tables 2 and 3 and Figure 1b.

(a) Geometries. The gas-phase geometry of $[BrOF_2][AsF_6]\cdot 2KrF_2$ optimized at C_1 symmetry at both levels of theory and did not deviate significantly from that observed in the X-ray crystal structure (Figure 1a). The largest angle discrepancies occur for F(3)---Br(1)---F(7) and Br(1)---F(7)−As(1), which are over- and underestimated, respectively, with respect to the experimental values (Figure 1b).

The calculated Br−O bond length was 1.556 (1.569) Å, and the Br−F bond lengths were 1.731 (1.757) Å and 1.730 (1.757)

(35) Bougon, R.; Bui Huy, T.; Charpin, P.; Gillespie, R. J.; Spekkens, P. H. *J. Chem. Soc., Dalton Trans.* **1979**, 6–12.
(36) Al-Mukhtar, M.; Holloway, J. H.; Hope, E. G.; Schrobilgen, G. J. *J. Chem. Soc., Dalton Trans.* **1991**, 2831–2834.
(37) Tavčar, G.; Tramšek, M.; Bunič, T.; Benkič, P.; Žemva, B. *J. Fluorine Chem.* **2004**, *125*, 1579–1584.
(38) Tramšek, M.; Žemva, B. *J. Fluorine Chem.* **2006**, *127*, 1275–1284.
(39) Turner, J. J.; Pimentel, G. C. *Science* **1963**, *140*, 974–975.

Å, in very good agreement with the experimental Br−O (1.564(5) Å) and Br−F (1.727(4), 1.723(4) Å) bond lengths. The calculated O−Br−F_1 (102.0 (102.0)°) and O−Br−F_2 (100.0 (100.1)°) angles are more open than the F−Br−F angle (89.1 (89.8)°), and all three bond angles are in good agreement with the experimental values. The three contact distances, Br---$F_{3,5,7}$, 2.350 (2.363) Å, 2.302 (2.338) Å, and 2.579 (2.529) Å, respectively, reproduce the observed distances (2.318(4), 2.356(4), 2.576(4) Å), with the contact opposite the oxygen atom, Br---F_7, being the longest.

The KrF_2 ligand geometries are also well modeled by the calculations, i.e., the bridging krypton−fluorine bond lengths, Kr−$F_{3,5}$, 1.951 (1.984) Å and 1.957 (1.984) Å, respectively, are longer than the terminal krypton−fluorine bond lengths, Kr−$F_{4,6}$, 1.814 (1.843) Å and 1.808 (1.837) Å, respectively. The KrF_2 ligands are also predicted to be near linear (177.2 (176.9)°, 177.5 (177.7)°), as observed experimentally.

The bond lengths, bond angles, and their trends for the pseudo-octahedral fluorine-bridged AsF_6^- anion are also well reproduced but not as well as for the cation. The arsenic−fluorine bridge bond length, As−F_7, 1.789 (1.813) Å, is elongated relative to the other As−F bonds. The remaining calculated As−F bond lengths range from 1.705 (1.720) Å to 1.761 (1.773) Å.

(b) Natural Bond Orbital (NBO) Analyses. The NBO[40−43] analyses were carried out for the PBE1PBE- and B3LYP-optimized gas-phase geometries of $[BrOF_2][AsF_6]\cdot 2KrF_2$ and KrF_2 with the results given in Table S3 in the Supporting Information. Both the PBE1PBE and B3LYP results are very similar; only the PBE1PBE results are referred to in the ensuing discussion.

The natural population analysis (NPA) charges given by the NBO analysis for Br (+2.41), O (−0.72), and F (−0.45) in the $BrOF_2^+$ cation of $[BrOF_2][AsF_6]\cdot 2KrF_2$ total +0.79 and are approximately half of the formal charges that are given by a purely ionic model (+5, −2, and −1, respectively), indicating that the cation bonds are polar covalent. The natural charges are also consistent with a cation having a net charge of +1 where the charge difference, −0.21, primarily arises from negative charge transfer from the KrF_2 ligands and, to a lesser extent from the AsF_6^- anion (−0.05), providing a total anion charge of −0.95. Of the plausible valence bond contributions that can be considered for the $BrOF_2^+$ cation (Structures I−IV), Structure IV best represents the calculated charges, the Br−O/Br-F bond order ratio (2.06), and Br/O/F/ valencies (2.27/0.95/0.46).

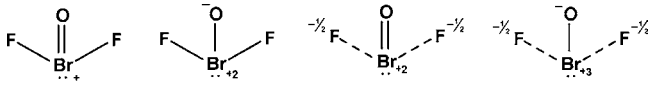

I II III IV

Among the three plausible valence bond structures for KrF_2, V, VI, and VII, the calculated charges (Kr 1.08, 1.08; F −0.58, −0.43, −0.58, −0.42), bond orders (0.24, 0.38, 0.25, 0.39), and valencies (Kr 0.64, 0.67; F 0.35, 0.39, 0.37, 0.40) of the coordinated molecules are best represented by $^{-1/2}$F---Kr^+---$F^{-1/2}$, the average of Structures VI and VII, which are customarily used to describe the bonding in KrF_2.[3] Upon adduct formation, the total of the fluorine atom charges of KrF_2 remains essentially unchanged; however, the charge distributions of the KrF_2 molecules are polarized toward the positive bromine atom, with ∼0.07 e transferred from F_t to F_b. A minor contribution from Structure VI accounts for the charge drift and also accounts for the decreased Kr−F_b bond order, increased Kr−F_t bond order, and increased F_t valence. In addition, upon coordination, the krypton atoms become somewhat more positively charged and there is an overall charge transfer of 0.08 e from each KrF_2 ligand to the $[BrOF_2][AsF_6]$ ion pair.

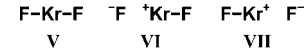

V VI VII

The valence bond description of $BrOF_2^+\cdot 2KrF_2$, which takes Structures IV and VI/VII into account, is represented by Structures VIII and IX, where Structure VIII is the dominant contributor and best accounts for the bonding in the adduct. A minor contribution from Structure IX accounts for the small increase in positive charge on the krypton atoms, the low Br−F_b bond orders (0.09, 0.10), and a small degree of charge transfer from the KrF_2 ligands.

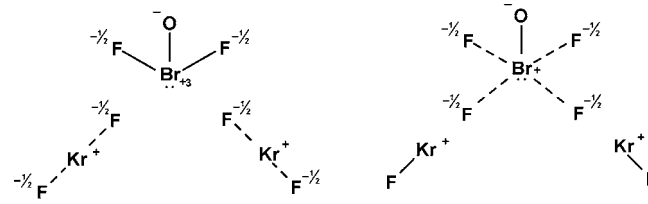

VIII IX

(c) QTAIM and ELF Analyses. The bonding was investigated by complementary use of the quantum theory of atoms in molecules (QTAIM)[44] and the topological analysis[45] of the Becke and Edgecombe electron localization function (ELF).[46] Both methods partition molecular space into adjacent nonoverlapping regions with the help of the gradient dynamical system theory, a technique very similar to that used in hydrology to determine drainage basins and drainage divides. An outline of QTAIM and ELF is provided in the Supporting Information. For the ensuing discussion, the following abbreviations denote atomic populations, $\bar{N}$(A); electron localization function, $\eta(\mathbf{r})$; core basins, C(A); valence basins, V(A, B, ...); monosynaptic basins, V(A); disynaptic basins, V(A, B); and closed isosurfaces, $\eta(\mathbf{r}) = f$, where f is defined as the isosurface contour. The QTAIM and ELF analyses of KrF_2, $BrOF_2^+$, and AsF_6^- fragments are provided in the Supporting Information.

Bonding in $[BrOF_2][AsF_6]\cdot 2KrF_2$. The NBO, AIM, and ELF bonding analyses provide a consistent picture of the reorganization of electron density that results from the formation of the KrF_2 complex, i.e., the net electron density transfer toward the $BrOF_2^+$ group and the polarization of the KrF_2 ligands. The very large electronegativity differences between $BrOF_2^+$ and KrF_2 (7.6 eV) and between $BrOF_2^+$ and AsF_6^- (14.2 eV), using

(40) Reed, A. E.; Weinstock, R. B.; Weinhold, F. *J. Chem. Phys.* **1985**, *83*, 735–746.
(41) Reed, A. E.; Curtiss, L. A.; Weinhold, F. *Chem. Rev.* **1998**, *88*, 899–926.
(42) Glendening, E. D.; Reed, A. E.; Carpenter, J. E.; Weinhold, F. *NBO Version 3.1*; Gaussian Inc.: Pittsburgh, PA, 1990.
(43) Glendening, E. D.; Badenhoop, J. K.; Reed, A. E.; Carpenter, J. E.; Bohmann, C. M.; Morales, C. M.; Weinhold, F. *NBO Version 5.0*; Theoretical Chemistry Institute, University of Wisconsin: Madison, WI, 2001.
(44) Bader, R. F. W. *Atoms in Molecules: A Quantum Theory*; Oxford University Press: Oxford, 1990.
(45) Silvi, B.; Savin, A. *Nature* **1994**, *371*, 683–686.
(46) Becke, A. D.; Edgecombe, K. E. *J. Chem. Phys.* **1990**, *92*, 5397–5403.

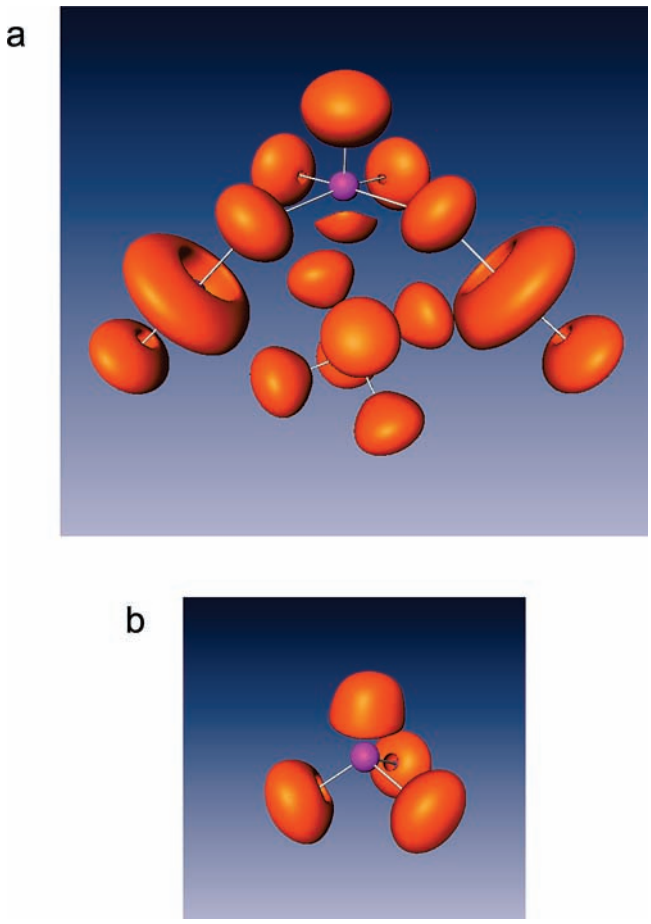

Figure 3. ELF localization domains for (a) $[BrOF_2][AsF_6]\cdot 2KrF_2$ compared with those of $BrOF_2^+$. The isosurface value is $\eta(\mathbf{r}) = 0.75$. Color code: magenta = core, brick-red = monosynaptic basin.

Parr's definition of electronegativity,[47] accounts for the direction of the charge transfer, whereas the hardness values[47] of KrF_2 (6.5 eV) and AsF_6^- (10.1 eV) account for the magnitudes of the contributions. The NPA and QTAIM populations provide global charge transfer values that are in agreement within a few hundredths of an electron. About 0.1 e is transferred from each KrF_2 and 0.05 e from AsF_6^-. In the complex molecular graph, the bromine atom is linked to the two bridging fluorines, F_3 and F_5, of the KrF groups and to F_7 of AsF_6^-. The values of the Laplacian of the electron density at the bond critical points are positive and decrease with the Br−F internuclear distance, i.e., 0.166 (Br−F_5), 0.157 (Br−F_3), and 0.122 (Br−F_7). Moreover, there is a degenerate critical point between Br and F_9. The delocalization indexes between Br and the weakly bonded fluorine atoms show almost the same trends: δ(Br, F3), 0.24; δ(Br, F_5), 0.22; δ(Br, F_7), 0.14; and δ(Br, F_9), 0.02. The localization domains of the complex at $\eta(\mathbf{r}) = 0.75$ are shown in Figure 3a, and the hierarchy of the ELF basins is given in Scheme 1. Although the bromine coordination number has increased to 6, the V(Br) ("valence electron lone pair on Br") basin population remains unchanged in the complex while its $\eta(\mathbf{r}) = 0.75$ localization domain appears to be contracted in the complex (Figure 3a) compared to that of the free $BrOF_2^+$ cation (Figure 3b).

(47) Parr, R. G.; Yang, W. *Density-Functional Theory of Atoms and Molecules*; Oxford University Press: Oxford, 1989; pp 90−98.

Scheme 1. Reduction of Localization Diagram for $[BrOF_2][AsF_6]\cdot 2KrF_2$ Showing the Ordering of Localization Nodes and the Boundary Isosurface Value, $\eta(\mathbf{r})$, at Which the Reducible Domains Split[a]

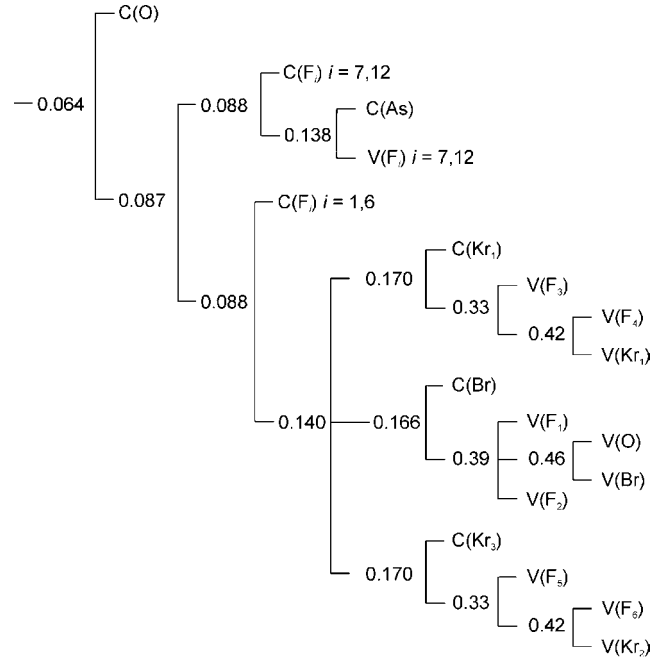

[a] The labeling scheme corresponds to that used in Figure 3a.

In fact, the V(Br) basin accommodates its shape and volume to the environment. In the complex it is confined within the cage formed by the F_1, F_2, F_3, F_5, and F_7 atoms, whereas there are no constraints in the free cation. In contrast to the classical AX_6E arrangement predicted by VSEPR rules,[25] the bond pair and electron lone pair arrangement around Br appears to be a hybrid of distorted octahedral, square pyramidal, and trigonal pyramidal geometries that are predicted for AX_6, AX_5E, and AX_3E arrangements. The angles subtended at bromine have the following values: O−Br−F_1, 102.0°; O−Br−F_2, 100.1°; O−Br−F_3, 90.7°; O−Br−F_5, 85.3°; O−Br−V(Br), 133.2°; and O−Br−F_7, 170.3°.

The deviations from the octahedral (or square pyramidal) value occur for those angles involving F_1 and F_2, which correspond to the shortest F−O internuclear distances (largest repulsions), and for F_7, which is close to the V(Br) basin. It is worth noting that the degenerate critical point mentioned above lies on a line linking F_9 to V(Br).

The interaction of the different groups also induces a redistribution of their electronic densities among their basins. The $BrOF_2^+$ cation attracts 0.25 e, which is almost equally distributed among the V(F) and V(O) basins, whereas the V(Br) population remains unchanged. In the AsF_6^- anion, the V(As, F) basins vanish in the complex and merge into the corresponding V(F) basins. Within the KrF_2 ligands, there is a density flow from the terminal fluorine and the krypton atomic basins toward the bridging fluorine whose net population is increased by 0.08 e. Paradoxically, the populations of the V(F_4) and V(F_6) basins increase with respect to the uncomplexed KrF_2 molecule at the expense of V(Kr). This polarization increases the covalent character of the Kr−F_4 and Kr−F_6 interactions; the Kr atomic basin contributions to V(F_4) and V(F_6) are 0.63 and 0.93 e, whereas the V(F_3) and V(F_5) basins only belong to the F_3 and F_5 atomic basins. This effect explains the contraction of the

$Kr-F_4$ and $Kr-F_6$ internuclear distances with respect to uncomplexed KrF_2.

Conclusion

The Lewis acid properties of the $BrOF_2^+$ cation and its resistance to oxidation have provided an avenue to the synthesis of a KrF_2 coordination complex with a main-group atom. The synthesis and crystal structure of $[BrOF_2][AsF_6]\cdot 2KrF_2$ provide a rare example in which KrF_2 functions as a ligand and represent a significant extension of krypton chemistry, accounting for much of what is presently known about the coordination chemistry of KrF_2. The vibrational assignments of the KrF_2 ligands and their descriptions substantiate those of known homoleptic XeF_2 coordination complexes with metal cations. The present findings may be expected to facilitate the extension of KrF_2 coordination chemistry to the syntheses of KrF_2 complexes with other main-group and metal centers.

The NBO, AIM, and ELF bonding analyses indicate that $[BrOF_2][AsF_6]\cdot 2KrF_2$ is organized around $BrOF_2^+$ and its stabilization is due to its Coulomb interaction with the AsF_6^- anion and to electron delocalization and charge transfers involving the KrF_2 ligands. This charge transfer increases the ionic character of the $Br-O$ and $Br-F_{1,2}$ bonds. The polarization of the KrF_2 ligands is a result of the electric field imposed by the $BrOF_2^+$ cation. Its main effect is to enhance the anionic character of each bridging fluorine atom, thereby giving rise to an electrostatic interaction with the positively charged bromine atom of the $[BrOF_2][AsF_6]$ ion pair. However, the stabilization energy is not large enough to enable significant local rearrangement of the ligands around the bromine atom, and consequently the two KrF_2 ligands are adjacent to one another. The study has provided two structurally related examples that illustrate strong ($BrOF_2^+$) and weak ($[BrOF_2][AsF_6]\cdot 2KrF_2$) valence electron lone pair behavior.[32]

Experimental Section

Apparatus and Materials. (a) General. All manipulations involving air-sensitive materials were carried out under strictly anhydrous conditions as previously described.[48] Reaction vessels, which also served as Raman sample tubes and NMR sample tubes, were fabricated from $^1/_4$-in. o.d. and 4-mm o.d. FEP tubing, respectively, and were outfitted with Kel-F valves. All reaction vessels and sample tubes were rigorously dried under dynamic vacuum prior to passivation with 1 atm of F_2 gas.

The starting material, $[BrOF_2][AsF_6]\cdot XeF_2$, was synthesized by solvolysis of $[XeOTeF_5][AsF_6]$ in BrF_5 as previously described.[49] Krypton difluoride was prepared and purified according to the literature method.[50] Anhydrous HF (Harshaw Chemicals Co.) was purified by the standard literature method.[51] High-purity Ar (99.998%, Air Liquide) or N_2 (obtained from liquid N_2 boil-off and dried by passage through a column of dry 3 Å molecular sieves) gases were used for backfilling vessels.

(b) $[BrOF_2][AsF_6]$. In a typical synthesis, 62.1 mg (0.126 mmol) of $[BrOF_2][AsF_6]\cdot XeF_2$ that had been prepared in a $^1/_4$-in. o.d. FEP reaction tube was pumped under dynamic vacuum for 12−18 h at 0 °C. The resulting white powder was shown to be $[BrOF_2][AsF_6]$ by low-temperature Raman spectroscopy[22] and, in contrast with a previous report,[22] was stable for at least 12 h at room temperature with no signs of decomposition.

(c) $[BrOF_2][AsF_6]\cdot 2KrF_2$. Approximately 0.3 mL of aHF was condensed into an evacuated $^1/_4$-in. o.d. FEP reaction tube containing 40.7 mg (0.126 mmol) of freshly prepared $[BrOF_2][AsF_6]$ at −196 °C. The frozen HF was melted onto the $[BrOF_2][AsF_6]$ sample at −78 °C and was then refrozen at −196 °C. Krypton difluoride (45.0 mg, 0.369) was sublimed into the reactor at −196 °C, followed by warming to −78 °C, whereupon KrF_2 immediately reacted as evidenced by the increased volume of the white solid that had remained undissolved at −78 °C. The reactants were well mixed, and the product was isolated after 2 h by removal of the HF solvent under dynamic vacuum at −78 °C.

X-ray Crystallography. (a) Crystal Growth. Crystals of $[BrOF_2][AsF_6]\cdot 2KrF_2$ were grown by a previously described procedure[52] that entailed slow cooling of an HF solution of $[BrOF_2][AsF_6]\cdot 2KrF_2$, previously saturated at ca. −40 °C, from −51 to −55 °C over the course of 5 h in a $^1/_4$-in. o.d. FEP reactor equipped with a side arm. When crystal growth had ceased, the reactor was maintained at −55 °C, and the supernatant was decanted into the side arm cooled to −78 °C. Once the majority of the supernatant had been decanted, the contents of the side arm were frozen at −196 °C, and the side arm was heat sealed off under dynamic vacuum. The crystals were dried under dynamic vacuum at −60 °C and stored at −78 °C until a suitable crystal could be selected and mounted at low temperature on the diffractometer.

(b) Crystal Mounting. The dried crystals were dumped into an aluminum trough cooled to -110 ± 5 °C by means of a cold stream of dry N_2 gas, allowing selection of individual crystals under a stereomicroscope as previously described.[53] A single crystal of $[BrOF_2][AsF_6]\cdot 2KrF_2$ was mounted at the tip of a glass fiber at -110 ± 5 °C using a Fomblin oil as the adhesive. The crystal used for data collection was a clear, transparent block measuring $0.20 \times 0.20 \times 0.18$ mm.

(c) Collection and Reduction of X-ray Data. The single crystal was centered on a SMART APEX II diffractometer, equipped with an APEX II 4K charge-coupled device (CCD) and a 3-axis goniometer, controlled by the APEX2 Graphical User Interface (GUI) software,[54] using graphite-monochromated Mo Kα radiation ($\lambda = 0.71073$ Å). The diffraction data collection consisted of a full ϕ-rotation (1010 frames collected at 0.36° intervals) at fixed $\chi = 54.74°$, followed by a series of short ω scans (250 frames) at various ϕ settings to fill the gaps. The crystal-to-detector distance was 4.959 cm, and the data collection was carried out in a 512×512 pixel mode using 2×2 pixel binning. Processing was carried out by using the APEX2 GUI software,[54] which applied Lorentz and polarization corrections to three-dimensionally integrated diffraction spots. The program SADABS[55] was used for scaling the diffraction data, the application of a decay correction, and an empirical absorption correction based on redundant reflections.

(d) Solution and Refinement of the Structures. The XPREP[56] program was used to confirm the unit cell dimensions and the crystal lattice. The structure was solved in the space group $P2_1/c$ by use of direct methods, and the solution yielded the positions of all the atoms. The final refinement was obtained by introducing anisotropic parameters for all the atoms, an extinction parameter, and the recommended weight factor. The maximum electron densities in the final difference Fourier maps were located around the bromine and krypton atoms. The PLATON program[57] could not suggest additional or alternative symmetries.

(48) Casteel, W. J., Jr.; Dixon, D. A.; Mercier, H. P. A.; Schrobilgen, G. J. *Inorg. Chem.* **1996**, *35*, 4310–4322.
(49) Keller, N.; Schrobilgen, G. J. *Inorg. Chem.* **1981**, *20*, 2118–2129.
(50) Chernick, C. L.; Malm, J. G. *Inorg. Synth.* **1966**, *8*, 254–258.
(51) Emara, A. A. A.; Schrobilgen, G. J. *Inorg. Chem.* **1992**, *31*, 1323–1332.
(52) Lehmann, J. F.; Dixon, D. A.; Schrobilgen, G. J. *Inorg. Chem.* **2001**, *40*, 3002–3017.
(53) Gerken, M.; Dixon, D. A.; Schrobilgen, G. J. *Inorg. Chem.* **2000**, *39*, 4244–4255.
(54) *APEX2*, release 2.0−2; Bruker AXS Inc.: Madison, WI, 1995.
(55) Sheldrick, G. M. *SADABS (Siemens Area Detector Absorption Corrections)*, version 2.10; Siemens Analytical X-ray Instruments, Inc.: Madison, WI, 2004.
(56) Sheldrick, G. M. *SHELXTL-Plus*, release 6.14; Siemens Analytical X-ray Instruments, Inc.: Madison, WI, 2000−2003.
(57) Spek, A. L. *J. Appl. Crystallogr.* **2003**, *36*, 7–13.

Raman Spectroscopy. Raman spectra were recorded on a Bruker RFS 100 FT-Raman spectrometer at −150 °C using 1064 nm excitation, 300 mW of laser power, and 1 cm^{-1} resolution as previously described with a total of 1200 scans acquired.[53]

Computational Results. The optimized geometry and frequencies of $[BrOF_2][AsF_6]\cdot 2KrF_2$ were calculated at the B3LYP and PBE1PBE levels of theory using aug-cc-pVTZ for all atoms. Pseudopotentials (aug-cc-pVTZ-PP) for Kr, As, and Br were used.[58] The combined use of aug-cc-pVTZ and aug-cc-pVTZ-PP is indicated as aug-cc-pVTZ(-PP).[58] The NBO analyses[40−43] were performed for the PBE1PBE and B3LYP optimized local minima. Quantum-chemical calculations were carried out using the program Gaussian 03[59] for geometry optimizations, vibrational frequencies, and their intensities. The program GaussView[60] was used to visualize the vibrational displacements that form the basis for the vibrational mode descriptions given in Table 3.

The QTAIM analysis can only be performed with the total density, which prevents the use of core pseudopotentials. The ELF approach also requires, in principle, the all-electron wave function, although small core pseudopotentials yield satisfactory results. For all of the studied systems, the all-electron wave functions have been calculated at the PBE1PBE/aug-cc-pVTZ optimized geometries with the DGDZVP basis set.[61] In order to validate the use of this basis set in the present topological analyses, the ELF populations and covariance matrix elements of KrF_2 were calculated at the PBE1PBE/aug-cc-pVTZ and PBE1PBE/DGDZVP levels and were compared. The numerical values of all basins involving the fluorine atoms agree within the numerical accuracy of the integration. There are small differences in the Kr basins because the descriptions of the inner shells are not identical (Table S4 in the Supporting Information). ELF grids and basin integrations have been computed with the TopMod package.[62,63] The ELF isosurfaces have been visualized with the Amira 3.0 software.[64]

Acknowledgment. We thank the Natural Sciences and Engineering Research Council of Canada for support in the form of a Discovery Grant (G.J.S.), the Ontario Graduate Scholarship in Science and Technology and the McMaster Internal Prestige "Ontario Graduate Fellowships" Programs for support in the form of scholarships (D.S.B.), and the computational resources provided by SHARCNet (Shared Hierarchical Academic Research Computing Network; www.sharcnet.ca).

Supporting Information Available: Complementary discussion of the X-ray crystal structure of $[BrOF_2][AsF_6]\cdot 2KrF_2$; factor-group analysis for $[BrOF_2][AsF_6]\cdot 2KrF_2$ (Table S1); experimental and calculated Raman frequencies for KrF_2 (Table S2); NBO valencies, bond orders, and NPA charges for $BrOF_2^+$, $[BrOF_2][AsF_6]\cdot 2KrF_2$, and KrF_2 (Table S3); outline of QTAIM and ELF; QTAIM and ELF analyses of KrF_2, $BrOF_2^+$, and AsF_6^- fragments; ELF localization domains of KrF_2 (Figure S1); ELF basin population and covariance matrix elements of KrF_2 (Table S4); ELF basin population, $\bar{N}[\Omega]$, covariance matrix elements, $\langle cov(\bar{N}[\Omega],\bar{N}[\Omega'])\rangle$, and bromine atomic basin contribution, $(\bar{N}[\Omega|Br])$, of $BrOF_2^+$ (Table S5); ELF localization domains for AsF_6^- (Figure S2); complete ref 59; and X-ray crystallographic file in CIF format for the structure determination of $[BrOF_2][AsF_6]\cdot 2KrF_2$. This material is available free of charge via the Internet at http://pubs.acs.org.

JA9098559

(58) Basis sets and pseudo-potentials were obtained from the Extensible Computational Chemistry Environment Basis set Database, version 2/25/04, as developed and distributed by the Molecular Science Computing Facility, Environmental and Molecular Science Laboratory, which is part of the Pacific Northwest Laboratory, P.O. Box 999, Richland, WA 99352.
(59) Frisch, M. J. et al. *Gaussian 98*, Revision A.11; Gaussian, Inc.: Pittsburgh, PA, 2003.
(60) *GaussView*, release 3.0; Gaussian Inc.: Pittsburgh, PA, 2003.
(61) Godbout, N.; Salahub, D. R.; Andzelm, J.; Wimmer, E. *Can. J. Chem.* **1992**, *70*, 560–571.
(62) Noury, S.; Krokidis, X.; Fuster, F.; Silvi, B. *Comput. in Chem.* **1999**, *23*, 597–604.
(63) Matito, E.; Silvi, B.; Duran, M.; Solà, M. *J. Chem. Phys.* **2006**, *125*, 024301.
(64) *Amira 3.0*; TGS, Template Graphics Software, Inc.: San Diego, CA, 2002.